PHYSICAL REVIEW A **84**, 060502(R) (2011)

Infrared spectrum of H_5^+ and D_5^+: The simplest shared-proton model

Cristina Sanz-Sanz, Octavio Roncero, Alvaro Valdés, Rita Prosmiti, Gerardo Delgado-Barrio, and Pablo Villarreal*
Instituto de Física Fundamental, IFF-CSIC, Serrano 123, E-28006 Madrid, Spain

Patricia Barragán
Centre Lasers Intenses et Applications (CELIA), Université de Bordeaux-I, UMR CNRS 5107 CEA, 351 Cours de la Libération, F-33045 Talence, France

Alfredo Aguado
Unidad Asociada UAM-CSIC, Departamento de Química Física, Facultad de Ciencias C-XIV, Universidad Autónoma de Madrid, E-28049 Madrid, Spain

(Received 3 October 2011; published 19 December 2011)

We present a two-dimensional collinear, adiabatic model to describe the motion of a proton in between two hydrogen molecules which adjust their elongation to trace a minimum-energy path. Together with bound states, the predissociative, vibrationally excited states involved in the electric dipole transitions are characterized. The main qualitative features of the infrared spectra of H_5^+ and its deuterated variant are discussed, and the effect of the temperature of the clusters is analyzed.

DOI: 10.1103/PhysRevA.84.060502 PACS number(s): 33.20.Ea, 33.20.Tp, 33.70.−w, 33.80.Gj

The $H_3^+ + H_2$ reaction, whose nuclear spin dependence has been very recently studied [1], has important implications for its use as an interstellar temperature probe [2] and its deuterated variants are among the most important reactions involved in deuterium fractionation in the interstellar medium [3]. Beside, infrared spectroscopic $H_5^+ + \hbar\omega \rightarrow H_3^+ + H_2$ measurements [4–6] provide information about the H_5^+ complex structure, energetics, and fragmentation dynamics. This last process can be viewed as a half collision, allowing a complementary study of the density of states involved in full collisions. Also, the rotational microwave spectra of the different isotopologues have been recently simulated [7] for their possible detection by the Atacama Large Millimeter Array (ALMA) observatory.

The delocalized and highly anharmonic shared-proton stretch mode was shown to carry very large oscillator strength, its excitation playing a major role in the assignment of experimental spectral features of H_5^+ and D_5^+ cations [6]. To date, several full dimensional potential energy surfaces (PESs) for H_5^+ are available [8–10]. In this Rapid Communication we use the accurate *triatomics in molecules* based analytical PES [9], fitted to high-level *ab initio* points [11], together with the electric dipole moment surface recently reported and used to perform spectra simulations at zero temperature [12]. To just account for the proton transfer between the two H_2 moieties, we present an extremely simplified two-dimensional (2D) model which incorporates the effect of the temperature.

Considering three collinear masses M_1-M_0-M_2, denoting by d_1 and d_2, the distances from the central mass to the extreme ones, and employing the coordinates $R = d_1 + d_2$ $(0 \leqslant R \leqslant \infty)$ and $r = d_1 - d_2$ $(-R \leqslant r \leqslant R)$ the kinetic energy operator in the center of mass system becomes

$$\hat{T} = -\frac{\hbar^2}{2}\left(\frac{1}{\mu_r}\frac{\partial^2}{\partial r^2} + \frac{1}{\mu_R}\frac{\partial^2}{\partial R^2} + \frac{2}{\mu_{rR}}\frac{\partial^2}{\partial r \partial R}\right), \qquad (1)$$

where

$$\frac{1}{\mu_r} = \frac{1}{\mu_{01}} + \frac{1}{\mu_{02}} + \frac{2}{M_0},$$
$$\frac{1}{\mu_R} = \frac{1}{\mu_{01}} + \frac{1}{\mu_{02}} - \frac{2}{M_0},$$
$$\frac{1}{\mu_{rR}} = \frac{1}{\mu_{02}} - \frac{1}{\mu_{01}},$$

with $\frac{1}{\mu_{0k}} = \frac{1}{M_0} + \frac{1}{M_k}$, $k = 1,2$. Labeling m as the hydrogen (deuterium) mass, we have $M_0 = m$, $M_1 = M_2 = 2m$, leading to $\mu_r = m/5$, $\mu_R = m$, and a vanishing crossed term in Eq. (1). The great difference of masses in these coordinates suggests to adiabatically separate the (fast) motion in r from the (slow) one in R, writing down the total wave function as $\Phi(r,R) \approx \phi_v(r;R)\psi_{v\epsilon}(R)$. Neglecting the derivatives with respect to R, the $\phi_v(r;R)$ functions fulfill the Schrödinger equation

$$\left[-\frac{5\hbar^2}{2m}\frac{\partial^2}{\partial r^2} + V(r,R) - W_v(R)\right]\phi_v(r;R) = 0, \qquad (2)$$

where V is the potential energy, while the R-dependent W_v eigenvalues drive the behavior of $\psi_{v\epsilon}$ and will be described below. There are residual coupling terms of the form

$$Q_{v'v}(R) = -\frac{\hbar^2}{2m}\left[2q^{(1)}_{v'v}(R)\frac{\partial}{\partial R} + q^{(2)}_{v'v}(R)\right], \qquad (3)$$

where $q^{(1)}_{v'v}(R) = \langle\phi_{v'}|\partial\phi_v/\partial R\rangle_r$, which vanishes for $v' = v$, and $q^{(2)}_{v'v}(R) = \langle\phi_{v'}|\partial^2\phi_v/\partial R^2\rangle_r$. They are calculated through the Hellmann-Feynman expression

$$q^{(1)}_{v'v}(R) = \frac{\langle\phi_{v'}|\frac{\partial V}{\partial R}|\phi_v\rangle_r}{W_v(R) - W_{v'}(R)}, \qquad (4)$$

and making use of the closure relationship,

$$q^{(2)}_{v'v}(R) = \sum_{v''\neq v'\neq v} q^{(1)}_{v'v''}(R)q^{(1)}_{v''v}(R). \qquad (5)$$

*p.villarreal@iff.csic.es

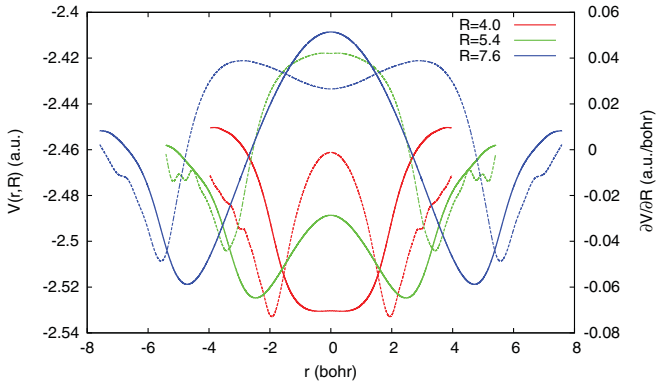

FIG. 1. (Color) Potential energy $V(r,R)$ (solid lines, left-hand vertical axis), and its derivative with respect to R (dashed lines, right-hand vertical axis), for three selected values of R (bohr).

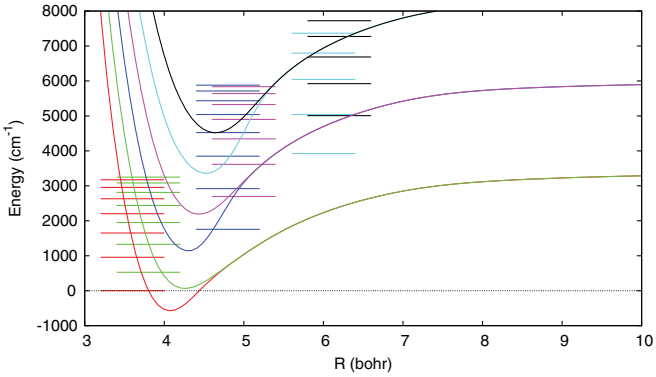

FIG. 2. (Color) H_5^+ adiabatic effective potentials $W_v(R)$ obtained by solving Eq. (6), and E_{vn} energy-level diagram.

The estimation of the derivative of the potential V in Eq. (4) constitutes a delicate task and hence it serves as a check of its softness.

Figure 1 displays the potential energy V of Ref. [9] at three values of R as a function of r. It was calculated fixing the system at a C_{2v} configuration with the two extreme H_2 perpendicular each to the other (see the $1C_{2v}$ structure depicted at Fig. 2 of Ref. [9]), allowing their bond lengths to adapt themselves to follow the minimum-energy path. For r near to zero, both H_2 interdiatomic distances are similar, but as long as r approaches the limits, the nearest diatomic stretches its bond length while the other shrinks it. In this way, and for each R, an asymmetric concerted vibration of the two diatomics takes place depending on the motion of the central particle. V is obviously r symmetric and evolves from an almost harmonic oscillator ($R < 4$ bohrs) to a double-well potential ($R > 5.4$ bohrs) through intermediate situations with increasing potential barriers centered at $r = 0$. The solutions of Eq. (2), even and odd states, also evolve from oscillator functions with well separated eigenvalues and a presence all along the box (small R values), to a spectrum at large R distances where each energy is doubly degenerate, with the proton being at one or other well without penetration into the region of the barrier. At large R the system corresponds to separated H_2 and H_3^+ species. Also in this figure the derivatives $\partial V/\partial R$ are depicted. Due to their symmetric character, only states of the same symmetry can be coupled through the kinetic terms mentioned above. Note the regular behavior of these derivatives in the region of interest, i.e., where the low-lying states are presumably located, although some oscillations become apparent near the limits of the corresponding box.

Thus, Eq. (2) describes the vibrations of the proton inside a box of length R, the distance between the two H_2 diatomics. The corresponding R-dependent eigenvalues $W_v(R)$ act as effective potentials to account for the stretching and shrinking of the box,

$$\left[-\frac{\hbar^2}{2m}\frac{d^2}{dR^2} + W_v(R) - \epsilon\right]\psi_{v\epsilon}(R) = 0. \tag{6}$$

For a given v, Eq. (6) shows discrete solutions ($\epsilon < W_v(R \to \infty)$, $\epsilon = E_{vn}$, $n = 0,1,\ldots$) as well as continuum ones [$\epsilon > W_v(R \to \infty)$].

For H_5^+, Fig. 2 displays the six low-lying effective potentials $W_v(R)$ obtained from Eq. (2). They correspond to even and odd ϕ_v states and become degenerate beyond $R \sim 5$ bohrs. Up to seven (discrete or quasidiscrete) levels appear to be sustained by them, showing a clear anharmonicity. Only those with $v < 2$, and also E_{20}, E_{21}, and E_{30}, are actually discrete. Note that the first excited level is E_{10}, the ground R state of the first asymmetric $v = 1$ manifold. Also note that only states of the same v symmetry can be coupled through residual kinetic terms, Eq. (3), which partially breaks some apparent degeneracies.

There are $\psi_{v'n'}$ excited states immersed in the continuum of $v'' < v'$ vibrational levels, $\psi_{v''\epsilon}$, which are coupled by the already mentioned kinetic terms $Q_{v''v'}$ of Eq. (3). Within a golden rule framework, the predissociation half-width associated with such excited states can be estimated as

$$\Gamma_{v'n'} = \pi \sum_{v''<v'} |\langle \psi_{v''\epsilon}|Q_{v''v'}(R)|\psi_{v'n'}\rangle_R|^2, \tag{7}$$

where the continuum wave functions $\psi_{v''\epsilon}$ are calculated on the energy shell, i.e., at $\epsilon = E_{v'n'} - W_{v''}(R \to \infty)$. As mentioned above, at large R values the system dissociates into H_2 and H_3^+ species, and ϵ represents the relative energy between these fragments.

The dipole moment surface $\mu(r,R)$ was also analytically fitted to the *ab initio* values [12]. At each R, it resembles a hyperbolic tangent as a function of r, that is, an odd function, and the corresponding transition dipole moments $\mu_{v'n';vn} = \langle \Phi_{v'n'}|\mu|\Phi_{vn}\rangle$ vanish unless the v', v states are of different symmetry. In order to account for the temperature, one considers a Boltzmann distribution over initial states. At a given temperature T, a line of intensity

$$I_{v'n',vn} \propto \frac{e^{-(E_{vn}/kT)}}{\sum_{v,n} e^{-(E_{vn}/kT)}}|\mu_{v'n';vn}|^2 \tag{8}$$

would appear at a frequency $\omega_{v'n',vn} = (E_{v'n'} - E_{vn})/\hbar$ of the incident photon. Continuum profiles are then obtained by

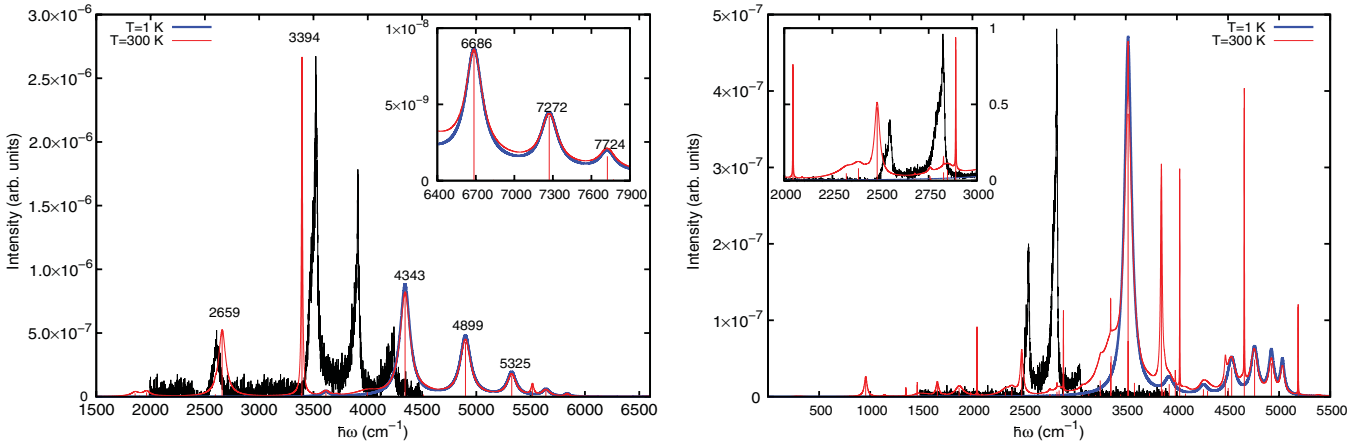

FIG. 3. (Color) ir spectra of H_5^+ (left-hand panel) and D_5^+ (right-hand panel) obtained at $T = 1$ and 300 K. They are compared to the experiments of Ref. [6]. The insets show the spectra at higher frequencies (H_5^+) and around the experimental main peaks (D_5^+).

dressing the above lines with Lorentzian functions of width $\Gamma_{v'n'}$ and summing up over transitions [13],

$$I(\omega) = \sum_{v'n'vn} \frac{\Gamma_{v'n'}/2\pi}{\hbar^2(\omega - \omega_{v'n',vn})^2 + \Gamma_{v'n'}^2/4} I_{v'n',vn}, \qquad (9)$$

fulfilling the condition $\int d\omega\, I(\omega) = \sum_{v'n'vn} I_{v'n',vn}$.

The left-hand panel of Fig. 3 displays ir absorption profiles obtained at $T = 1$ and 300 K for H_5^+. From the appealing progression of the calculated bands at $T = 1$ K, and since the present dissociation energy $D_0 = W_0(R \to \infty) - E_{00} =$ 3449 cm^{-1} is overestimated with respect to the 7D value of 2415 cm^{-1} [12], one might consider a redshift of ∼1000 cm^{-1} of the whole profile to match with the experiment [6], which is also depicted. However, the discrepancy between the simple 2D model and accurate calculations could not be restricted to dissociation energies affecting also the shape of adiabatic potentials and the location of excited states in a rather complicated manner. At $T = 300$ K, the emerging profile conserves the features coming from the (0,0) initial state (which now contributes with 92% from the Boltzmann distribution), but additional bands appear at the region of lower frequencies due to population of the (1,0) and (0,1) states (7% and 1%, respectively). The corresponding transition energies, intensities, and predissociation half-widths are collected in the left-hand part of Table I. The profile accords with the experimental bands placed at 2603, 3520, and 4232 cm^{-1} (see Ref. [6]), and differences of ∼100 cm^{-1} could be attributed to low frequencies associated with rotations of H_2 which are not accounted for by the model. The band placed at 3904 cm^{-1} is missing, while undetected decreasing bands beyond 4500 cm^{-1} do appear. In the inset of this figure we show the profile in the region of 6400–7900 cm^{-1}, which has also been reported [5]. There is good accord with the experiment with regard to the peaks at 6690, 7130, and 7770 cm^{-1}, although the band detected at 7490 cm^{-1} is missing. As a matter of fact, the band at 3904 cm^{-1} was assigned to the (ν_1) H_2 stretch band [4] (3910 cm^{-1} in that reference), and that at 7490 cm^{-1} to the overtone ($2\nu_1$) [5], which obviously is not accounted for in the present model. Including relative intensities, the agreement with the experiment is excellent. Predissociation half-widths [half-width at half maximum (HWHM)] in the region below 6000 cm^{-1} are close to the Gaussian broadening of 30 cm^{-1} assumed in the simulations of Cheng *et al.* [6] and similar to the ones obtained by wave-packet calculations [12], although with orders of magnitude larger than those previously reported [14]. We should mention that according to the laser bandwidth used in the experiments, half-widths lower than 1 cm^{-1} have been neglected, i.e., the corresponding transitions do not contribute to the spectrum. In the upper region, they are in the range 70–80 cm^{-1} (see Table I) with the experimental estimation by Bae [5] being 50 cm^{-1} (FWHM = 100 cm^{-1}).

TABLE I. Main contributing transitions $v,n;v',n'$ to the H_5^+ (left-hand part) and D_5^+ (right-hand part) ir spectra. ΔE: frequencies (cm^{-1}); I: intensities (10^{-6} a.u.) at $T = 300$ K; and Γ: predissociation half-widths (cm^{-1}). For frequencies, the closest experimental data peaks [5,6] are included in parentheses.

$v,n;v',n'$	ΔE	I	$\Gamma_{v'n'}$	$v,n;v',n'$	ΔE	I	$\Gamma_{v'n'}$
1,2;2,2	1898	4.1	137	3,1;4,1	956	1.3	16
0,2;3,1	1963	4.0	38	2,1;5,1	2045	0.3	1
0,1;3,1	2659	61	38	1,1;4,1	2482	2.9	16
	(2603)				(2546)		
1,0;4,0	3394	49	6	2,0;5,1	2890	0.4	1
	(3520)				(2815)		
0,0;3,1	3614	4.4	38	0,0;3,3	3522	49	42
1,0;2,3	3996	15	119	1,0;4,2	3848	7.8	9
	(3904)						
0,0;3,2	4343	140	54	0,0;3,4	3926	2.8	53
	(4232)						
0,0;3,3	4899	78	58	0,0;5,1	4027	1.0	1
0,0;3,4	5325	26	48	0,0;3,5	4260	1.5	50
1,0;4,2	5517	3.8	14	0,0;3,6	4536	5.5	46
0,0;3,5	5640	5.9	39	0,0;5,2	4660	1.8	1
0,0;3,6	5836	1.1	18	0,0;3,7	4760	5.9	39
0,0;5,2	6686	1.6	78	0,0;3,8	4924	4.1	30
	(6690)						
0,0;5,3	7272	0.8	79	0,0;3,9	5053	2.6	23
	(7130)						
0,0;5,4	7724	0.3	73	0,0;5,3	5186	0.6	1.5
	(7770)						

Because of the mass effect, D_5^+ presents deeper W_v potentials, albeit analogous to those shown in Fig. 2, and a more congested spectrum than H_5^+. Hence, the 2D adiabatic model could be less suitable. ir absorption profiles at $T = 1$ and 300 K are displayed in the right-hand panel of Fig. 3 together with the experiment [6]. The corresponding detailed data are listed in the right-hand part of Table I. When one moves from $T = 1$ to 300 K, a similar effect as the already mentioned for H_5^+ is obtained, i.e., unique features at lower excitation energies arise. The population of the (0,0) level at 300 K decreases to 80%, the rest being more widely distributed among excited states, although the whole profile is similar at the two temperatures. The more intense band remains at 3522 cm^{-1}, and with the exception of some additional narrow features, the structured profile at higher energies which comes from excitations of the (0,0) ground level is almost unchanged. However, the additional features appearing at $T = 300$ K approach the experimental data. The region of frequencies of 2000–3000 cm^{-1} is enlarged in the inset of the figure, where the intensity is normalized to the maximum of the experimental peak. With the exception of a narrow peak at 2045 cm^{-1} which does not appear in the experiment, the bands placed at 2482 and 2890 cm^{-1} are similar to the experimental ones at 2542 and 2815 cm^{-1}.

In summary, we have presented a simple model which accounts for the proton transfer in H_5^+ and D_5^+ and incorporates the temperature effect. The present assignments are no longer associated with the individual frequencies of the H_3^+ or H_2 moieties, and are only based on the shared-proton motion. Although some features of the ir spectrum of H_5^+ could be explained by considering a global redshift at very low temperatures, simulations at room temperatures reproduce much better the experimental data. For D_5^+, as a consequence of its larger mass, the model might become less suitable and only a partial accord with the experiment is attained at $T = 300$ K. For the two species, and independently of the temperature, the model predicts several intense bands at higher frequencies than those recently detected [6]. We think that further experimental measurements would assist in clarifying the present findings.

Michael A. Duncan is deeply acknowledged for providing us his experimental results. This work has been supported by the Consolider-Ingenio 2010 Programme CSD2009-00038 (MICINN), MICINN Grant No. FIS2010-18132, and CAM Grant No. S-2009/MAT/1467. P.B. acknowledges support from the "Fundación Ramón Areces." The aid of COST Action CM1002 (CODECS) is also appreciated.

[1] K. N. Crabtree, C. A. Kauffman, B. A. Tom, E. Beka, B. A. McGuire, and B. J. McCall, J. Chem. Phys. **134**, 194311 (2011).

[2] K. N. Crabtree, N. Indriolo, H. Kreckel, B. A. Tom, and B. J. McCall, Astrophys. J. **729**, 15 (2011).

[3] T. J. Millar, A. Bennett, and E. Herbst, Astrophys. J. **340**, 906 (1989).

[4] M. Okumura, L. I. Yeh, and Y. T. Lee, J. Chem. Phys. **88**, 79 (1988).

[5] Y. K. Bae, Chem. Phys. Lett. **180**, 179 (1991).

[6] T. C. Cheng, B. Bandyopadyay, Y. Wang, S. Carter, B. J. Braams, J. M. Bowman, and M. A. Duncan, J. Phys. Chem. Lett. **1**, 758 (2010).

[7] B. A. McGuire, Y. Wang, J. M. Bowman, and S. L. W. Weaver, J. Phys. Chem. Lett. **2**, 1405 (2011).

[8] Z. Xie, B. J. Braams, and J. M. Bowman, J. Chem. Phys. **122**, 224307 (2005).

[9] A. Aguado, P. Barragán, R. Prosmiti, G. Delgado-Barrio, P. Villarreal, and O. Roncero, J. Chem. Phys. **133**, 024306 (2010).

[10] P. Barragán, R. Prosmiti, O. Roncero, A. Aguado, P. Villarreal, and G. Delgado-Barrio, J. Chem. Phys. **133**, 054303 (2010).

[11] R. Prosmiti, P. Villarreal, and G. Delgado-Barrio, J. Phys. Chem. A **107**, 4768 (2003).

[12] A. Aguado, C. Sanz-Sanz, P. Villarreal, and O. Roncero (submitted to Phys. Rev. A, 2011).

[13] D. López-Durán, M. P. de Lara-Castells, G. Delgado-Barrio, P. Villarreal, C. Di Paola, F. A. Gianturco, and J. Jellinek, Phys. Rev. Lett. **93**, 053401 (2004).

[14] V. Ŝpirko, T. Amano, and W. P. Kraemer, J. Chem. Phys. **124**, 244303 (2006).